

PROPAGATION OF WIDEBAND SIGNALS IN SHALLOW WATER IN THE PRESENCE OF MESO-SCALE HORIZONTAL STRATIFICATION

Boris Katsnelson¹, Andrey Malykhin² and Alexandr Tckhoidze¹

¹School of Marine Sciences, University of Haifa, 31905, Israel

²Physics Department of Voronezh University, Voronezh, 394006, Russia

katz@phys.vsu.ru

In the paper examples of an oceanic waveguide with parameters varying in the horizontal plane are considered: an area of coastal wedge, (slopes and canyons), an area of varying water layer properties - in the presence of nonlinear internal waves and a temperature front. In these cases there is significant horizontal refraction or redistribution of the sound field in the horizontal plane. Due to waveguide dispersion (dependence of modal propagation constants on frequency) the refraction index in the horizontal plane depends on frequency also, and it is possible to observe different spatial and temporal variations of the sound signal similar to those in a two dimensional medium with frequency and spatial dispersion. This can be manifested as a non-stationary interference pattern, arrival time variations, and/or variations of spectra. These effects can be used to solve different inverse problems especially by using horizontal and vertical line arrays.

INTRODUCTION

In most publications concerned with sound propagation in shallow water authors have concentrated on the vertical variability of the temperature field, and discussed a simple model of how that variability arises. This vertical structure is the most important feature of the shallow water column, as the water column and bottom are approximately horizontally stratified (comprised of vertically stacked layers) over the propagation scales of interest, which reach to about 50 km in shallow water. However, horizontal stratification is a broad-brush first approximation only, and in many shallow water scenarios there is appreciable sound speed variability in the horizontal direction, as well as in the vertical. Perhaps the strongest horizontal variability in shallow water is due to shallow water fronts and bathymetry variations, mainly in areas of the coastal wedge and nonlinear internal waves. In this paper we consider just three types of horizontal variability.

TEMPERATURE FRONT

Figure 1 shows the configuration of the Polar front in the Barents Sea [1]. The temperature variation is non-uniform in depth: as a rule, it is concentrated in the vicinity of the thermocline.

Aforementioned temperature variations are accompanied by a change in the sound speed profile, which is most pronounced across the front. In the vicinity of the thermocline, the sound speed drop across the front can reach 15–20 m/s within a distance of several hundreds of metres. Such a difference corresponds to a substantial horizontal sound speed gradient, which persists over a rather large area. More detailed information on the temperature front is presented in Figure 2: it shows a sequence of sound speed profiles when passing from one side of the temperature front to another in a region of the

Barents Sea within a zone of about 500 m in length where the temperature variations are most pronounced [1,2].

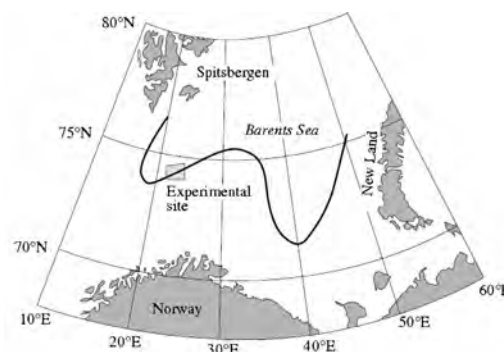


Figure 1. Temperature front (Barents Sea Polar front)

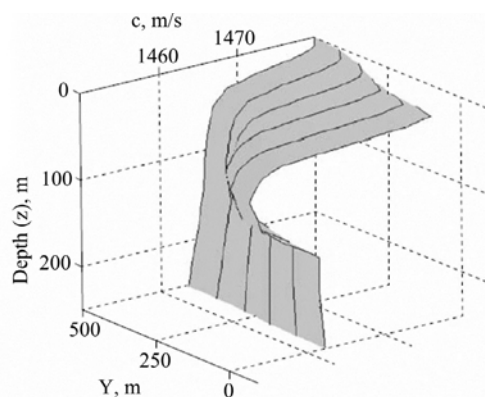


Figure 2. Sequence of sound speed profiles in the vicinity of the temperature front. The nearest and farthest profiles correspond to the colder Arctic Current and the North-Atlantic Current, respectively

Under the influence of such a gradient, the oceanic medium becomes acoustically anisotropic, and a number of effects arise in the course of sound propagation through it. In particular, space–time fluctuations of the sound field due to the modes coupling in the region where the acoustic path crossed the Polar front of the Barents Sea were considered in [1,2]. Another effect that can considerably change the sound field is the horizontal refraction, which manifests itself when the acoustic path is approximately parallel to the TF. The approach of horizontal rays and vertical modes can be applied to such a phenomenon. Such a study can reveal a number of spatial and frequency–time effects that, in principle, can be experimentally observed by using a vertical hydrophone array. In this sense, the influence of the temperature front on the sound field is similar to that of soliton-like internal waves (or internal solitons (IS)) [3], although the horizontal gradients of the sound speed in the TF are 2–5 times lower than those in the IS, and the velocities of the TF are much smaller than those of the IS.

Let us consider the space–frequency features of the sound field propagating in a shallow-water sound channel with a temperature front. The oceanic medium is represented as a three-dimensional underwater waveguide in the Cartesian coordinate system where the (X,Y) plane coincides with the sea surface and the Z axis is directed vertically downwards. The waveguide is formed by the water layer $0 \leq z \leq H$ with density $\rho(x,y,z) = \rho_0(z) + \delta\rho(y,z)$ and a sound speed profile $c(x,y,z) = c_0(z) + \delta c(y,z)$, where $\rho_0(z)$ and $c_0(z)$ correspond to the profiles of density and sound speed on one side of the TF. In our case, δc and $\delta\rho$ characterise the variations of the acoustic parameters under the influence of the TF. The latter is considered to be plane and parallel to the X axis. The bottom is assumed to be homogeneous, liquid, and absorbing with density ρ_1 , sound speed c_1 and absorption coefficient α . Here, the TF is modelled in such a way that, on average, the temperature (and the sound speed as well) at $y > 0$ is higher than that at $y < 0$ (see Figure 2). Correspondingly, the horizontal rays leaving the source at $y < 0$ will be refracted in the same direction (Figure 3). In other words, our statement of the problem corresponds to the situation where, at the receiving array positioned in the zone of intersection of horizontal rays, a complicated structure will be observed as the result of interference of the direct horizontal ray with a set of horizontal rays deflected by the temperature gradient and corresponding to different horizontal angles at the source and different vertical modes. The particular characteristic of the horizontal refraction is that the horizontal rays corresponding to different frequencies and different vertical modes propagate along different trajectories, and, consequently, the intensity of the sound field at the reception point may depend on the frequency and the ordinal number of the detected mode

First of all, one can estimate the distance from the source and the temperature front, or, in other words, the position of the zone where one can expect the intersection of the direct and refracted horizontal rays and, hence, the manifestations of the aforementioned phenomena. Specifically, such a zone that is closest to the source is determined by the maximum admissible departure angle β of the horizontal ray that returns to the region $y < 0$ after its refraction in the zone of the temperature front. In the simplest case, the estimate is as follows [5]:

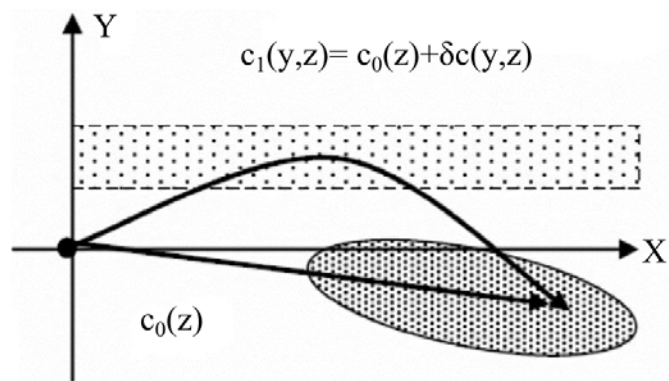


Figure 3. Schematic diagram of the horizontal refraction in the region near the temperature front. The shaded area is the zone of probable enhancement of the sound field due to horizontal refraction. The dashed strip approximately indicates the transition layer

$$\beta \approx \sqrt{2 \frac{h_t}{H} \frac{\delta c}{c}} \quad (1)$$

where h_t is the thickness of the thermocline. For the Barents Sea [1], $H \sim 230$ m, $h_t \sim 70$ – 90 m, $\delta c \sim 15$ – 20 m/s, and, hence, $\beta \approx 6$ – 8×10^{-2} . This means that, if the source is at a distance of 600–800 m from the temperature front with a thickness of about 500 m, the effects of horizontal refraction manifest themselves at the receiver that is at a distance of about 20 km along the temperature front.

INTERNAL WAVES

Intense internal waves (IWs) are known to cause substantial perturbation of the low-frequency sound field. The well-known study [4] reports on measuring the fluctuations of the sound field over a horizontal array in the presence of IWs with the propagation path passing at a small (about 10°) angle to the wave fronts of a train of intense IWs moving along the coastline. It was experimentally established that the amplitude fluctuations of the sound field correlated with the fluctuations of the water layer influenced by IWs. Data from numerical simulation allow one to assume the adiabatic mechanism of interaction between the IWs and the sound field: the intensity variations are caused by local changes in the waveguide parameters. A detailed study of fluctuations of the sound field under the influence of IWs was also performed in the SWARM'95 experiment [6] for different orientations of the acoustic path with vertical receiving arrays used for mode filtering. Publications [7–9] devoted to analysing the data of the SWARM'95 experiment show that, when the acoustic path is approximately parallel to the wave front of the IW train, intensity fluctuations can be rather substantial because of the influence of horizontal refraction. A theoretical analysis and estimation of intensity fluctuations were presented in [9] in the framework of a ray approximation in the horizontal plane. There, in terms of horizontal rays, the mechanism of intensity fluctuations was explained by changes in the ray density (the cross-section of the ray tube). In this case, the estimates of intensity variations can be obtained by assuming the

horizontal rays to be approximately straight with perturbations of the phase front being neglected. On the other hand, in the presence of appreciable horizontal refraction, the objective of the study is to consider the fluctuations of the directions of sound propagation in the horizontal plane (the fluctuations of the phase front in a more general formulation). For instance, an experiment measuring the fluctuations of the direction of sound propagation in the horizontal plane was carried out in the Barents Sea [10]. There, a horizontal hydrophone array was used to study the fluctuations in the phase distribution with characteristic periods starting from several tens of minutes, which, according to the authors, correspond to the typical periods of IWs.

In the present paper we estimate the variations of the sound-field phase front under the effect of a train of intense internal waves crossing the acoustic path and consider the possibility of experimental observation of such variations.

An illustration of the influence of internal waves on sound propagation is shown in Figure 4 where there is a 3D shallow-water sound channel with IWs. The ocean medium is represented as an underwater waveguide in the XYZ coordinate system, where the XY plane coincides with the sea surface and the Z axis is oriented vertically downwards. The waveguide is formed by a water layer $0 \leq z \leq H$ with a density $\rho(z)$ and a sound speed profile $c(x,y,z) = c_0(z) + \delta c(x,y,z,T)$, where $c_0(z)$ corresponds to the equilibrium stratification of the layer and $\delta c(x,y,z,T)$ characterises the changes of the acoustic properties of the layer under the influence of IWs. The latter quantity depends on both coordinates and time T (we make a difference between the “slow” time T that characterises the variability in δc and “quick” time t , determining sound field variability)

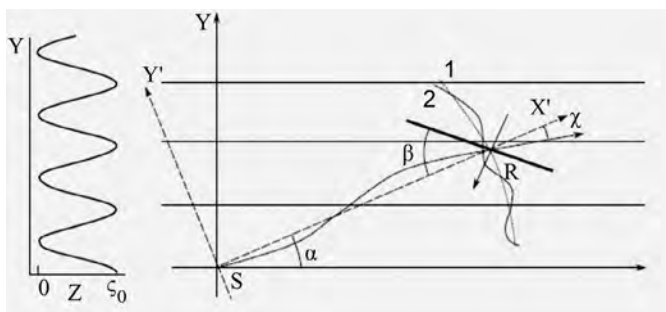


Figure 4. The XY coordinate system is related to IWs, the $X'Y'$ coordinate system is determined by the direction of the acoustic path, α is the angle between the path and the wave front of IWs, β is the angle between the path and the array, and γ is the angle of horizontal refraction. At the left, the position of the IW envelope is shown at the instant $T = 0$. The (1) dotted and (2) solid curves show the wave front without and with IWs, respectively

Let us consider an IW train with an approximately rectilinear wave front that is parallel to the X axis and with an envelope depending on the y coordinate and with an amplitude ζ_0 . This train propagates along the Y axis with a speed v . The sound source S is located at the origin of coordinates in the horizontal plane $x = y = 0$ at a depth $z = z_1$. The transmitted signal is received at the observation point $R(x,y,z)$ by a horizontal array (usually $z = H$). The initial position of the IW envelope at $T = 0$

is such that the IW’s maximum is at the source at the zero shift of the train, $vT = 0$ (the envelope with amplitude ζ_0 is shown in the left-hand part of Figure 4). Because of the slow propagation of the IW train, the characteristics of the sound field will depend on the position of the train, or on time T , in a parametric manner. For brevity, we do not write this dependence in an explicit form.

COASTAL WEDGE

In the ocean, coastal slope regions are of primary importance for both practical purposes and research, including acoustic studies. A typical coastal slope region has the form of a wedge with the angle between the sea surface and the bottom reaching $\sim 0.005\text{--}0.01\text{rad}$; this region extends for several tens of kilometres (or more) from the coast to the shelf edge, where the sea depth is about 200–350 m. Beyond this line, the sea depth begins to increase steeply (the continental slope). In the theoretical studies of sound propagation, the coastal slope is usually described by a wedge shaped model region with a constant velocity of sound and with ideally or non ideally reflecting boundaries [11–14]. The solution to the problem of the field in an ideal wedge can be constructed by using, e.g. imaginary sources, in analogy with the well known Pekeris model; in this case, the imaginary sources are positioned in a circle [11, 14]. In some papers the field in the wedge is constructed in a cylindrical coordinate system (the z axis coincides with the edge of the wedge) based on modes depending on angle ϑ in the vertical plane. A somewhat different approach is possible in the case of a smooth dependence of the sea depth on the distance to the coast (a small slope), when the wedge-shaped region can be considered as a waveguide with varying depth and, in terms of the depth dependent field expansion in modes, the field can be described in the adiabatic approximation (ignoring the mode coupling). In the two-dimensional version of the problem, where the field only varies in the vertical plane, one of the main features of sound propagation up the slope is the appearance of the critical cross section for a mode of a fixed number at a fixed frequency with decreasing depth and the reflection of this mode; or, the transformation of the mode into a leaky one and, hence, its escape into the bottom at a certain distance from the edge, this distance being different for different modes and frequencies [15]. The three-dimensional problem was considered in studies of the horizontal refraction of the acoustic field in a coastal slope region in both experimental (laboratory experiments [16] and full-scale experiments in a coastal slope region [17]) and theoretical investigations. In the latter, the field behaviour was described in terms of vertical modes and horizontal rays or numerically [18] by a parabolic equation (see references in [18]). For the ideal wedge model, the ray equations in the horizontal plane have analytic solutions describing the position and shape of rays and caustics in the form of hyperbolas [19]. In the case of a wedge with ideally reflecting surfaces, two rays (the direct ray and the refracted) arrive at each of the points of the horizontal plane, and the corresponding interference pattern is formed. We note that, for a more realistic model (a non-ideal bottom and/or a coordinate dependent sound velocity), the field pattern is more complicated, especially with allowance for the dependence of the refractive index of horizontal rays

on frequency and vertical mode number. Sound propagation in the horizontal plane is similar to the propagation in an inhomogeneous dispersive medium with similar features for narrowband and broadband signals. A similar situation occurs to that in the vicinity of the temperature front [5].

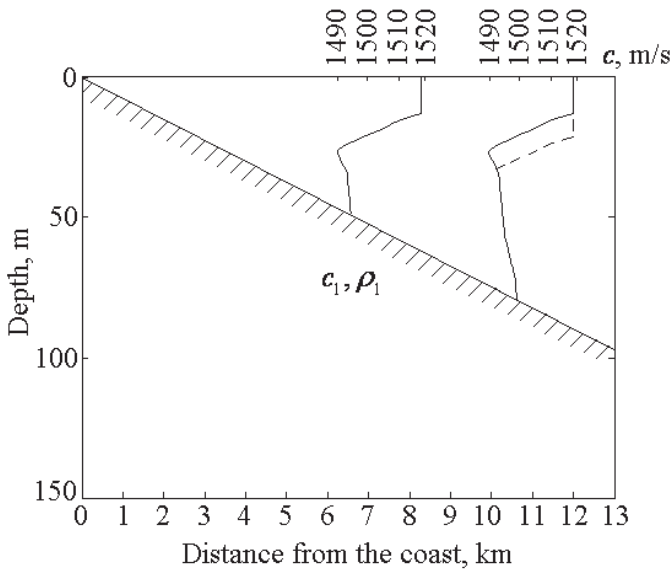


Figure 5. Bathymetry and sound velocity profiles for the waveguide model under study. The dashed line shows the perturbed sound velocity profile under mesoscale perturbation

THEORY OF THE SOUND FIELD IN A HORIZONTALLY STRATIFIED WAVEGUIDE

The complex sound field amplitude of a point source characterised by spectrum $S(\omega)$ and positioned at a point with the coordinates is sought in the form

$$P(\vec{r}, z, t) = 2 \int_0^{\infty} \sum_l P_l(\vec{r}, \omega) \psi_l(\vec{r}, z; \omega) e^{-i\omega t} d\omega \quad (2)$$

Here, $\psi_l(\vec{r}, z; \omega)$ is the eigenfunction with the number l ; it is determined by the Sturm–Liouville problem and includes the dependence on r (or (x, y)) as a parameter; and in addition, depends on frequency. The quantity $P_l(\vec{r}, \omega)$ which depends on the horizontal coordinates, the sound frequency, and the source coordinates, can be called the spectral mode amplitude.

We denote the corresponding eigenvalue (the longitudinal wavenumber) by $q_l(\vec{r}, \omega)$. For the value $P_l(\vec{r}, \omega)$ neglecting mode coupling we can get the two dimensional Helmholtz equation:

$$\nabla_{\perp}^2 P_l(\vec{r}, \omega) + q_l^2(\vec{r}, \omega) P_l(\vec{r}, \omega) = 0 \quad (3)$$

where $\nabla_{\perp}^2 = \frac{\partial^2}{\partial x^2} + \frac{\partial^2}{\partial y^2}$ is the Laplace operator in the horizontal plane.

Instead of the eigenvalue $q_l(\vec{r}, \omega)$, which determines the space and time dependences of the wavenumber for sound propagation in the horizontal plane, we introduce the corresponding mode refractive index $n_l(\vec{r}, \omega) = q_l(\vec{r}, \omega) / q_1^0$ where q_1^0 is the eigenvalue of the transverse Sturm–Liouville

problem; this eigenvalue corresponds to the cross section at a certain fixed point, e.g., at the point of the source position. We note that, in the region lying between the source and the coast ($y < y_s$), the wavenumber is $q_l < q_1^0$ and $(n_l(\vec{r}, \omega) < 1)$. For a real situation, the latter index differs little from unity $n_l(\vec{r}, \omega) < 1 - \delta n_l, |\delta n_l| \ll 1$.

Figures 6 and 7 show the value of the increment for our models of temperature front and wedge as a function of the distance to the front and to the edge of the wedge for different frequencies and mode numbers. One can see that, in the region $y < y_s$, the increment increases with an increase in the mode number and with a decrease in frequency; i.e., the refractive index increases with increasing frequency.

The frequency dependence of the refractive index makes the two-dimensional propagation medium a dispersive one (Eq. (3)). For such a medium, the evolution of the sound signal in time is determined by Eq. (2). If the spectrum of the emitted signal is sufficiently narrow, we can ignore the frequency dependence (which is sufficiently smooth) of the eigen functions within this spectrum; then, we factor out the eigen functions from under the integral in Eq. (2) at the central frequency ω_0 of the source spectrum. In this case, the signal amplitude takes the form

$$P(\vec{r}, z, t) = 2 \sum_l \psi_l(\vec{r}, z; \omega_0) \int_0^{\infty} P_l(\vec{r}, \omega) e^{-i\omega t} d\omega = \sum_l \psi_l(\vec{r}, z; \omega_0) P_l(\vec{r}, t) \quad (4)$$

where the quantity $P_l(\vec{r}, t)$ can be interpreted as the pulse amplitude of the l^{th} mode. As usual for space-time ray approximation we find

$$P_l(\vec{r}, t) = A_l(\vec{r}, t) e^{i\Theta(\vec{r}, t)} \quad (5)$$

where phase (eikonal) depending on coordinates and time can be found by different ways [19, 20]. Examples of variations in refractive index in the horizontal plane for a wedge and temperature front are shown in Figures 6 and 7.

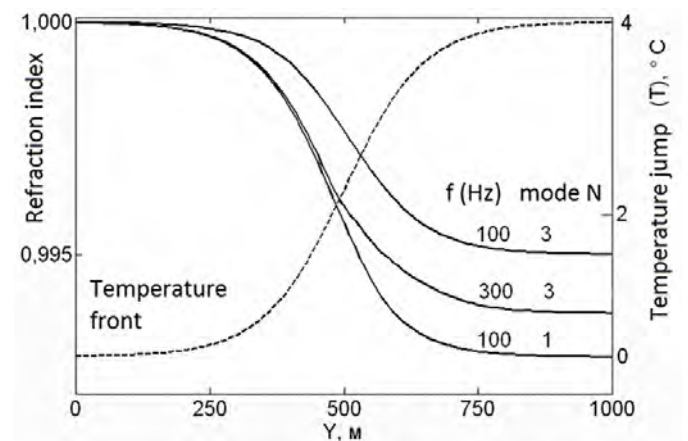


Figure 6. Dependence of the refractive index of the horizontal rays on the Y coordinate for some frequencies and mode numbers in the region of the temperature gradient. The dashed curve indicates the variation of temperature at some depth in the thermocline region across the temperature front

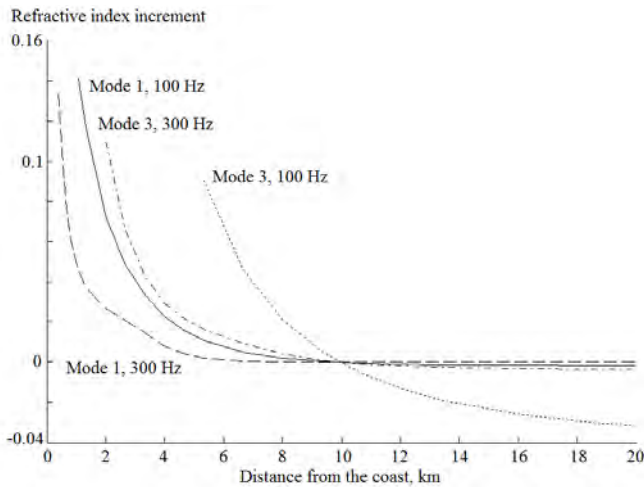


Figure 7. Dependence of the refractive index increment on the distance to the edge of the wedge for different modes and frequencies (the values are indicated in the plot)

STRUCTURE OF HORIZONTAL RAY PATTERN

If we take all the values $0 < t < \infty$, the corresponding curve will determine the spatial horizontal rays. Figure 8 shows examples of horizontal rays in the area of the temperature front. In Figure 9 we can see pattern of horizontal rays in the area of the coastal wedge for a frequency of 100 Hz, which corresponds to the first mode. In the plot, the multipath region can be distinguished. Its shape resembles a sector, so that, in what follows, we use the term “multipath sector” (MS). When the receiver is located in the MS, one should observe the interference of the direct and reflected fields of the corresponding modes if the overlapping of signals arriving over different ray paths takes place or if signal doubling occurs with a certain time interval in the case of pulse arrival time measurements. The interference pattern is rather complicated because of the presence of regions where only one mode (the first) propagates or only two modes propagate (e.g., the first and second modes), and so on. The lower boundary of the sector, i.e., the boundary closest to the coast, represents the caustics (envelope) for the horizontal rays corresponding to a given mode and a given frequency, and the upper (limiting) horizontal ray indicates the MS boundary farthest from the coast.

The positions of the boundaries can be estimated on the basis of a three-dimensional ray consideration with the use of the Brillouin (vertical) grazing angle β_l for the l^{th} mode. The upper limiting ray path in the horizontal plane, or the horizontal launch angle of the boundary ray, which is denoted by $\bar{\chi}_l$ (see Figure 9(a)) and determines the aforementioned ray path, is governed by the parameters of the bottom or, more precisely, by the angle of total internal reflection from the bottom.

As the ray propagates from the source, both the horizontal angle and the Brillouin angle of the given mode (the vertical grazing angle with respect to the bottom) β_l vary (Figure 9(b)). In other words, during propagation up the slope the channel narrows, and the angle decreases, whereas the vertical grazing

angle β_l , which depends on the local depth of the channel, increases and, at a certain instant, may become identical to the angle of total internal reflection from the bottom which depends on c_l . In this case, the direct ray penetrates to the bottom and the reflected (or refracted) ray is absent. The corresponding horizontal ray launch angle (see Figure 9(a)) is determined as follows. The local eigenvalue corresponding to total internal reflection, or the related bottom grazing angle of the Brillouin ray belonging to the l^{th} mode is determined by the expression $\cos \bar{\beta}_l = \bar{q}_l / k = c(\bar{H}) / c_l$ where \bar{H} is the sea depth at the turning point. This yields the refractive index at the turning point for the horizontal boundary ray: $n_l = \bar{q}_l / q_l^0 = k_1 / q_l^0$ where $k_1 = \omega / c_l$ and the horizontal angle χ_l at the turning point is zero. Then $\bar{\chi}_l$ is determined by the relation $\cos \bar{\chi}_l = k_1 / q_l^0$. The corresponding boundary ray path is shown in Figure 9(a). Now, we estimate the coordinates of the ray turning point (\bar{x}_l, \bar{y}_l) , which approximately coincides with the vertex of the MS under the assumption that the sound velocity in the wedge is constant. In this case, the horizontal ray paths and ray caustics have the form of hyperbolas [5], whose equations are obtained in an analytic form. Using these results, for the coordinates of the vertex of the hyperbola corresponding to the boundary ray, we derive

$$\bar{x}_l = y_0 \frac{\sin \bar{\chi}_l \cos \bar{\chi}_l \cos^2 \beta_l^0}{1 - \cos^2 \bar{\chi}_l \cos^2 \beta_l^0} = y_0 \frac{k_1 \sqrt{(q_l^0)^2 - k_1^2}}{k^2 - k_1^2}$$

$$\bar{y}_l = y_0 \frac{\sin \beta_l^0}{\sqrt{1 - \cos^2 \bar{\chi}_l \cos^2 \beta_l^0}} = y_0 \frac{\sqrt{k^2 - (q_l^0)^2}}{\sqrt{k^2 - k_1^2}} \quad (6)$$

For our bottom model (the parameters are given above), we can assume that, in the denominator of Eq. (10), $q_l^0 \sim k$; then, we have $\bar{x}_l y_0 k_1 / \sqrt{k^2 - k_1^2} \sim 2y_0 \sim 20$ km. We see that \bar{x}_l weakly depends on both mode number and frequency. The coordinate \bar{y}_l exhibits a more pronounced dependence on the mode number, as well as on frequency. For example, for the second mode at a frequency of 100 Hz, from Eq. (10) we obtain $\bar{y}_l \sim 0.5, y_0 \sim 5$ km. In general, the straight line $y = \bar{y}_l$ determines the boundary beyond which the l^{th} mode does not propagate (at the given frequency).

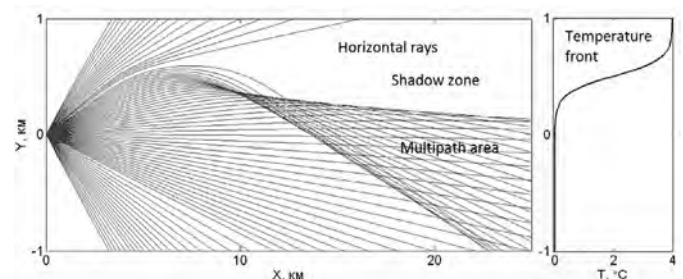


Figure 8. Ray pattern calculated by using the method of vertical modes and horizontal rays with the corresponding temperature distribution at some depth (at the right) in the vicinity of the temperature front for the first vertical mode at a frequency of 300 Hz

TIME-FREQUENCY DIAGRAM AND WIDEBAND PULSE PROPAGATION

The eikonal (the phase) taken at a certain point of the horizontal plane is determined by the phase velocity and the corresponding integral along the horizontal ray from the point of radiation to the point of reception (observation):

$$\Theta_l(M,t) = \int_{R_{0M}} q_l(x,y) ds \quad (7)$$

The characteristic features of the pulse arrival time are illustrated in Figure 10, where, together with the horizontal ray pattern for the first and third modes at a frequency of 200 Hz, one can see lines lying in the horizontal plane, which correspond to a constant arrival time $t = 45s$ for signals propagating along the respective ray paths. The regions are denoted as follows: (I) the shadow zone for all modes, (II) the multipath region for the first mode and the shadow zone for the third mode, (III) the multipath region for the first and the third modes, and (IV) the region of only the direct ray paths of these modes. One can see that, in the multipath regions, for each of the modes, there are two curves $t_l(x,y) = \text{const}$ corresponding to the direct and reflected signals. The signal propagating over the direct ray path goes farther within a fixed time interval as compared to the ray arriving over the reflected ray path. In other words, for a fixed point in the multipath region, the direct signal usually arrives earlier than the reflected signal; the difference decreases with decreasing distance to the caustics where the direct and reflected rays coincide. The time of signal propagation over the ray path (which is an important observation characteristic) is determined by the integral along the ray path

$$t_l(\omega) = \int_{R_{0M}} \frac{ds}{v_l^{gr}(x,y;\omega)} \quad (8)$$

where $v_l^{gr}(x,y;\omega)$ is the group velocity of the l^{th} mode, depending on coordinates along ray path. Comparing the arrival times at the reception point for different modes, we see that, in the absence of horizontal refraction (for the direct horizontal rays), a “conventional” order of mode arrivals is observed: the lower modes are usually characterized by a higher group velocity, and their travel time is shorter. For the reflected signals in region III, a different order of mode arrivals takes place. This change in arrival order is related to the fact that, despite the higher group velocity of mode 1, as compared to mode 3, the difference in the lengths of the respective ray paths is such that the order of arrival is changed. In particular (see Figure 10), for the direct signal, the first mode arrives before the third mode (in regions III and IV), whereas, for the reflected signals (region III), the third mode arrives before the first one.

Let us consider in more detail the signal arrival time at the observation point, which may fall within the MS. First of all we remark that arrival times can be different for different horizontal rays coming to the receiver. Typical values of arrival times are shown in Figure 11 for a temperature front. Experimental observation of this effect was published in [21] for a moving front of internal waves.

Next we consider arrival times, as a function of frequency for different vertical modes (Figure 12). The corresponding

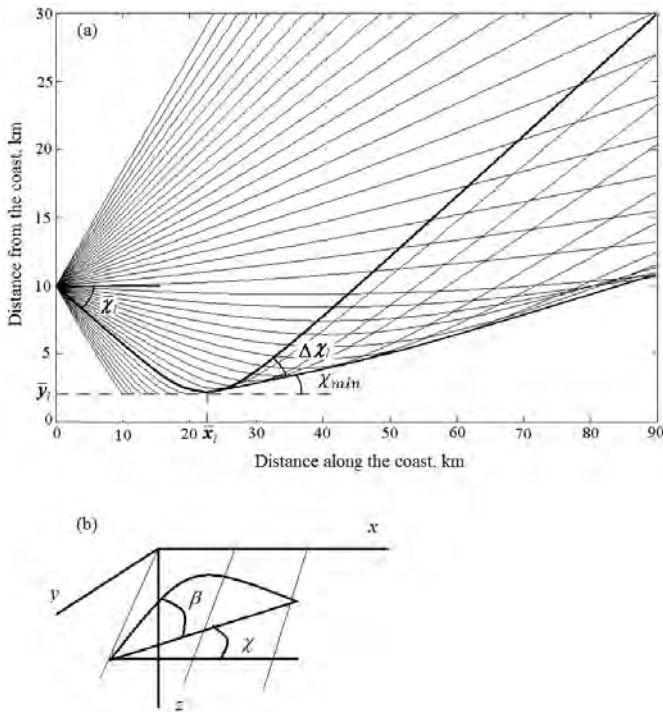


Figure 9. (a) Horizontal ray pattern for the first vertical mode at a frequency of 100 Hz; the solid lines indicate the MS. (b) The vertical and horizontal angles for a three-dimensional ray

One can see that the numerically calculated position of the MS vertex approximately coincides with the coordinates determined above. If we assume that, for our wedge model, the caustic approximately coincides with the asymptote of the corresponding hyperbola (the caustic for the case of a constant velocity), the slope of this asymptote is $\tan \beta_l^0$ i.e. its angle with the x axis is β_l^0 . This angle noticeably increases with increasing mode number. The asymptote of the “upper” horizontal boundary ray has the slope $dy/dx = \sqrt{k^2 - k_l^2} / k_l$ which, in the framework of the simple model, is the same for different modes and frequencies and only depends on the sound velocities in water and in the bottom. In the case under consideration, the aforementioned estimate yields a slope of ~ 0.53 or an angle $\chi_l \sim 30^\circ$, which approximately coincides with the numerical results represented in Figure 9(a). In Figure 9(a), the direction of the lower boundary is determined by the angle χ_{\min} , which in our case approximately coincides with β_l^0 ; for the first mode at a frequency of 100 Hz, this angle is $\chi_{\min} \sim 5^\circ - 6^\circ$. The vertex angle of the sector is estimated as $\Delta\chi_l \sim \chi_l - \chi_{\min}$ and decreases with the mode number. We note that, as the mode number increases and the frequency decreases, the increment of the horizontal refractive index δn_l increases and the MS shifts toward greater depths. In this case, the characteristic spatial dimensions of the region vary (the transverse size of the MS at a distance of ~ 30 km makes about 2–4 km). As the frequency increases, the angle χ_{\min} decreases (tends to zero) and the lower boundary of the MS shifts toward the coast for all of the modes.

pattern is called the frequency–time diagram and is often plotted in theoretical considerations and on the basis of experimental data [22]. This pattern reveals the shapes of the dispersion curves for individual modes and is used for solving various problems [23]. The position of the observation point used in our calculations is shown in Figure 10 (its approximate coordinates are $x = 50$ km, $y = 4.5$ km). From Figure 12 one can see that, for frequencies $\omega < \omega_1$ where $\omega_1 = 100$ Hz, the receiver falls within the shadow zone for all of the modes. As the lower boundary of the MS shifts toward the x axis and the receiver falls within the caustic for the first mode; here $\omega = \omega_1$, the direct and reflected rays coincide and the corresponding signals arrive simultaneously. With a further increase in frequency $\omega > \omega_1$ the lower boundary of the MS shifts further and falls within the MS for the first mode (still remaining in the shadow zone for the second mode); in this case, two signals are observed with the interval between the first mode arrivals over the direct and reflected ray paths increasing with frequency (the characteristic time between the direct and reflected signal arrivals is ~ 0.5 s). This corresponds to zone II in Figure 10. As the frequency increases, the signal travel time decreases for the direct ray (the group velocity increases with frequency) and increases for the reflected ray (because of the predominant increase in the ray path length). When the frequency reaches the value $\omega = \omega_2 \approx 250$ Hz, the second mode appears at the observation point and the situation is reproduced. For a fixed mode number, as the frequency increases further, the observation point may fall outside the multipath region (we denote the corresponding frequency value as $\omega = \bar{\omega}_l$) and, in this case, only one signal arrives at the observation point. Note that the specific values of ω_l and $\bar{\omega}_l$ depend (in addition to the dependence on the waveguide parameters and the mode number) on the position of the observation point in the horizontal plane. The situation where the observation point falls outside the MS is only possible when this point lies in a relatively narrow region near the upper boundary (see Figure 9). Such a frequency–time diagram can be plotted in an experiment with the use of broadband signals (a frequency band of about 50–500 Hz). It is also possible to consider the spectral features of the signal and, in particular, the spectrum of the received signal as a function of the receiver position. These features are determined by the frequency dependence of the horizontal ray paths.

Let's consider propagation of the wideband pulse. In the presence of horizontal stratification due to the frequency dependence of the refractive index in the horizontal plane each Fourier component of the pulse will propagate along a different trajectory joining source and receiver. In the Figure 13(a) two horizontal rays, corresponding to frequencies of 100 and 300 Hz are shown in the vicinity of the temperature front (refractive index is shown in the Figure 13(b)). It means, first of all, that the frequency spectrum of the received signal will be different in comparison with what would be received in the absence of horizontal refraction, due to a different phase shift for each Fourier component. Next, for different trajectories (Fourier components) we have different directions of wave vectors (tangent to horizontal rays) in the horizontal plane both at the locations of the source and receivers. For example in the

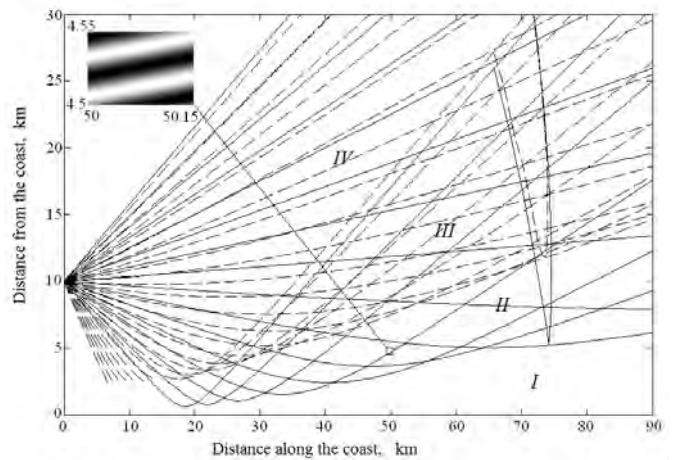


Figure 10. Set of horizontal rays for the first (the solid lines) and fourth (the dashed lines) vertical modes. The frequency is 200 Hz. The lines lying in the horizontal plane and corresponding to a signal arrival time of 45s are indicated. The inset shows the interference pattern formed in the horizontal plane segment near the point indicated in the plot.

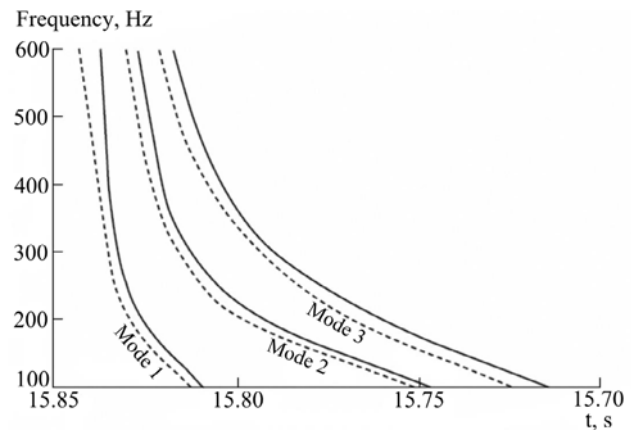


Figure 11. Arrival times for horizontal rays reflected from temperature front

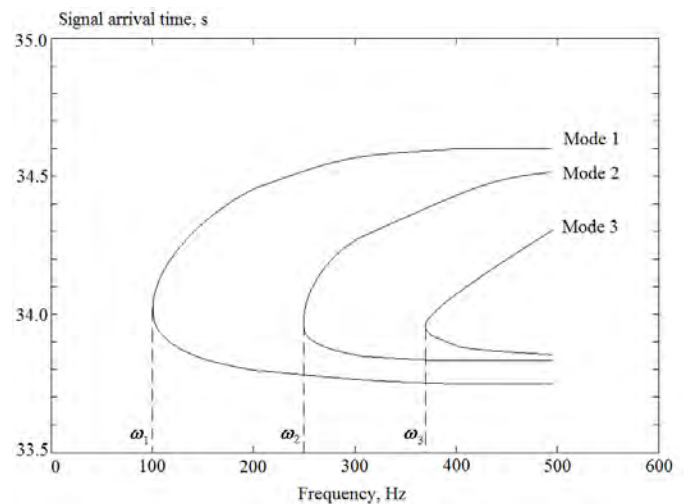


Figure 12. Frequency–time curves for three modes. The numbers are indicated in the plot.

situation corresponding to Figure 13 angles between mentioned vectors at the source are about 3° , and at the receiver $\sim 2^\circ$. In other words we can say that for the sound field near the receiver there is a dependence $\vec{q}_l = \vec{q}_l(\omega)$, that is similar to a medium with spatial dispersion. One of the consequences of this with broadband signals will be spatial modulation of the interference pattern across the direction of propagation and different directions of group and phase velocities.

An example of the interference pattern formed by the beam containing two frequencies, 100 and 300 Hz, in the vicinity of the receiver (Figure 13) is shown in Figure 14(b). We see that in comparison with Figure 14(a) (absence of frequency dependence for horizontal rays) there is spatial modulation of the interference pattern in the y-direction. The scale of this modulation can be estimated as $\Lambda \sim 2\pi/|\Delta\vec{q}|$, where $\Delta\vec{q}$ is the difference between wave vectors, corresponding to frequencies in the beam. We see that in the Figure 14(b) the scale of variability in the y-direction is a few hundreds of metres, in accordance with the angle between vectors for 100 and 300 Hz.

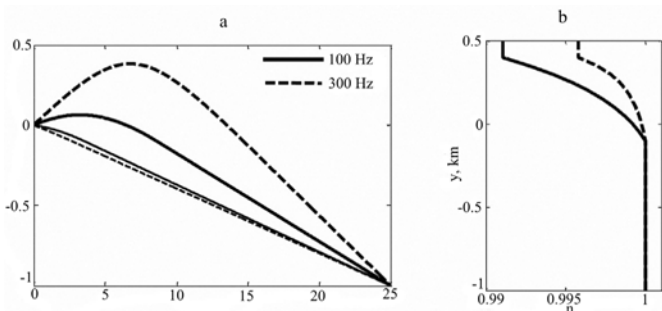


Figure 13. (a) - Horizontal rays (vertical mode 1), frequencies 100 and 300 Hz (direct and reflected from the front). (b) - refractive index n in the horizontal plane for mentioned frequencies

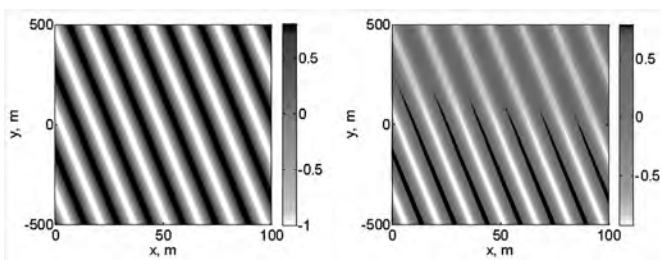


Figure 14. Interference pattern in the vicinity of the receiver neglecting frequency dependence of horizontal rays (left panel) and taking into account frequency dependence

CONCLUSION

We can conclude that the existence of anisotropic meso-scale perturbations can lead to different acoustical effects, such as redistribution of the sound field in the horizontal plane, variation of the spectrum of the signal and a change of temporal shape of a received pulse. Next, due to the frequency dependence of the trajectory of horizontal rays it is possible to observe effects similar to spatial dispersion in sound propagation. All these effects occur in situations considered

in the paper, however different spatial scales of coastal wedge (for example) and nonlinear internal waves produce different values of acoustical parameters: horizontal angles, arrival times, interference pattern in the horizontal plane. This implies that to observe these effects it is necessary to take different distances between source and receivers as well as distances from wave fronts and coast lines. It is also necessary to use vertical and horizontal line arrays, allowing different sorts of filtering to be carried out.

ACKNOWLEDGMENTS

Work was supported by BSF, grant 2010471, and RFBR grant 12-05-00887.

REFERENCES

- [1] G. Jin, J.F. Lynch, C.S. Chiu and J.H. Miller, "A theoretical and simulation study of acoustic normal mode coupling effects due to the Barents sea Polar Front, with applications to acoustic tomography and matched-field processing", *Journal of the Acoustical Society of America* **100**(1), 193-205 (1996)
- [2] J.F. Lynch, G. Jin, R. Pawlowicz, D. Ray, A.J. Plueddemann, C.S. Chiu, J.H. Miller, R.H. Bourke, A.R. Parsons and R. Muench, "Acoustic travel-time perturbations due to shallow-water internal waves and internal tides in the Barents Sea Polar front: Theory and experiment", *Journal of the Acoustical Society of America* **99**(2), 803-821 (1996)
- [3] B.G. Katsnelson, A.Y. Malykhin and A.V. Tskhoidze, "Rearrangement of the horizontal space-time structure of the sound field in shallow water in the presence of moving internal waves", *Acoustical Physics* **57**(3), 368-374 (2011)
- [4] D. Rubenstein and M.N. Brill, "Acoustic variability due to internal waves and surface waves in shallow water", in *Ocean Variability and Acoustics Propagation*, eds. J. Potter and A. Warn-Varnas, Kluwer Academic, 1991, pp. 215-228
- [5] B.G. Katsnelson, J.F. Lynch and A.V. Tskhoidze, "Space-frequency distribution of sound field intensity in the vicinity of the temperature front in shallow water", *Acoustical Physics* **53**(5), 611-617 (2007)
- [6] J.R. Apel, M. Badiéy, C.S. Chiu, S. Finette, R.H. Headrick, J. Kemp, J.F. Lynch, A. Newhall, M. H. Orr, B. H. Pasewark, D. Tielberger, A. Turgut, K. von der Heydt and S.N. Wolf, "An overview of the 1995 SWARM shallow-water internal wave acoustic scattering experiment", *IEEE Journal of Oceanic Engineering* **22**, 465-500 (1997)
- [7] M. Badiéy, Y. Mu, J.F. Lynch, J.R. Apel and S.N. Wolf, "Temporal and azimuthal dependence of sound propagation in shallow water with internal waves", *IEEE Journal of Oceanic Engineering* **27**(1), 117-129 (2002)
- [8] M. Badiéy, B.G. Katsnelson, J.F. Lynch, S.A. Pereselkov and W.L. Siegmann, "Measurement and modeling of three-dimensional sound intensity variations due to shallow-water internal waves", *Journal of the Acoustical Society of America* **117**(2), 613-625 (2005)
- [9] M. Badiéy, B.G. Katsnelson, J.F. Lynch and S. Pereselkov, "Frequency dependence and intensity fluctuations due to shallow water internal waves", *Journal of the Acoustical Society of America* **122**(2), 747-760 (2007)
- [10] A.Y. Shmelerv, A.A. Migulin and V.G. Petnikov, "Horizontal refraction of low-frequency acoustic waves in the Barents Sea stationary acoustic track experiment", *Journal of the Acoustical Society of America* **92**(2), 1003-1007 (1992)

- [11] G.B. Deane and M.J. Buckingham, "An analysis of the three-dimensional sound field in a penetrable wedge with a stratified fluid or elastic basement", *Journal of the Acoustical Society of America* **93**(3), 1319-1328 (1993)
- [12] F.B. Jensen and W.A. Kuperman, "Sound propagation in a wedge-shaped ocean with a penetrable bottom", *Journal of the Acoustical Society of America* **67**(5), 1564-1566 (1980)
- [13] A.D. Pierce, "Guided mode disappearance during upslope propagation in variable depth shallow water overlying a fluid bottom", *Journal of the Acoustical Society of America* **72**(2), 523-531 (1982)
- [14] E.K. Westwood, "Broadband modeling of the three-dimensional penetrable wedge", *Journal of the Acoustical Society of America* **92**(4), 2212-2222 (1992)
- [15] M.J. Buckingham, "Theory of three-dimensional acoustic propagation in a wedgelike ocean with a penetrable bottom", *Journal of the Acoustical Society of America* **81**(2), 198-210 (1987)
- [16] C.T. Tindle, H. Hobaek and T.G. Muir, "Downslope propagation of normal modes in a shallow water wedge", *Journal of the Acoustical Society of America* **81**(2), 275-286 (1987)
- [17] R. Doolittle, A. Tolstoy and M. Buckingham, "Experimental confirmation of horizontal refraction of cw acoustic radiation from a point source in a wedge-shaped ocean environment", *Journal of the Acoustical Society of America* **83**(6), 2117-2125 (1988)
- [18] F. Sturm, "Numerical study of broadband sound pulse propagation in three-dimensional oceanic waveguides", *Journal of the Acoustical Society of America* **117**(3), 1058-1079 (2005)
- [19] L.M. Brekhovskikh and Y.P. Lysanov, *Fundamentals of ocean acoustics*, Springer-Verlag, New York, 2003
- [20] Y.A. Kravtsov and Y.I. Orlov, *Geometrical optics of inhomogeneous media*, Springer, Berlin, 1990
- [21] M. Badiey, B. Katsnelson, Y-T Lin and J. Lynch, "Acoustic multipath arrivals in the horizontal plane due to approaching nonlinear internal waves", *Journal of the Acoustical Society of America* **129**(4), EL141-147 (2011)
- [22] C. Chen, J.H. Miller, G.F. Bourdreaux-Bartels, G.R. Potty and C.J. Lazauski, "Time-frequency representations for wideband acoustic signals in shallow water", *Proceedings of Oceans 2003*, **5**, pp. 2903-2907, September 2003
- [23] M. Lopatka, G. Le Touzé, B. Nicolas, X. Cristol, J.I. Mars and D. Fattaccioli, "Underwater broadband source localization based on modal filtering and features extraction", *EURASIP Journal on Advances in Signal Processing*, 2010:304103 (2010)



Portable Solutions for **Sound & Vibration Analysis**

REALWAVE POCKET ANALYSER

Ideal for measuring and analysing

- general sound and vibration
- environmental noise
- construction and blast sound and vibration
- architectural acoustics
- ship vibration

Powerful analysis in the palm of your hand

- Real time FFT analysis
- Spectrograms
- FFT based octave analysis
- Digital filter based octave analysis
- Vibration level meter with human vibration filter
- Sound level meter
- FFT based RPM meter
- 1, 2, 3 and 4 channel models available



HW Technologies

www.hwtechnologies.com.au